Numerical Study on Heat Reduction of Various Counterflowing Jets over Highly Blunt Cone in Hypersonic Flow

M. Barzegar Gerdroodbary[1] and M. A. Fayazbakhsh[2]
[1]Department of Mechanical Engineering, Iran University of Science & Technology, Narmak, Tehran 16844, Iran

[2]School of Engineering Science, Simon Fraser University, Surrey, BC, Canada

Abstract
In this paper, the effectiveness of counterflowing jets as heat-reduction devices for large-angle blunt cones flying at hypersonic Mach numbers is numerically simulated with various coolant jets. Different jet conditions have been chosen to investigate the effect of the counterflow jet on the surrounding flow field of nose cone. The compressible, unsteady, axisymmetric Navier-Stokes equations are solved with SST turbulence model for free stream Mach number of 5.75 at 0° angle of attack with and without gas injection. The coolant gas (air, Carbon Dioxide, and helium) is chosen to inject into the hypersonic flow at the nose of the model. The numerical results presented the surface heat reduction for different coolant jets. According to the investigation of various conditions of opposing jets, important phenomena of flow field and some effective jet conditions are found.

Keywords: Heat Flux Reduction; Hypersonic flow; Numerical Analysis; Counterflowjets, Freestream-Jet Interactions.

1. INTRODUCTION

The efficiency and performance of any air vehicle is dictated by the physics of the flowfield of the vehicle and/or propulsion system. The flowfields of supersonic and hypersonic vehicles and propulsion systems are characterized by strong shock systems, which may include different types of shocks: oblique (forebody, inlet) shocks, normal shocks and other shock structures and interactions. For a given geometry, the strength of the shocks increases with increasing flow Mach number. Strong shocks contribute disproportionately to the drag of the vehicle, and may cause severe aerothermal loads, which could translate into poor aerodynamic performance (lift/drag) and stringent thermal protection system requirements, i.e. severe penalties in vehicle range and weight, etc., for single- or two-stage transatmospheric cruise and reentry vehicles.

Concepts to enhance the aerodynamic and aerothermal performance of supersonic and hypersonic vehicles by weakening the shock system are not new. Various techniques such as concentrated energy deposition along the stagnation streamline, retractable aerospikes ahead of the blunt body, forward-facing jets in the stagnation zone of a blunt body, and also supersonic projectiles fired in the upstream direction from the stagnation zone are being evaluated by many research groups around the world to keep the heating of the blunt body below acceptable levels during its atmospheric ascent [1–6]. Also, several numerical simulations are recently done in order to analyze the resulting flow field of each technique [7–9].

In recent years, there has been a strong interest in using weakly ionized nonequilibrium plasma (WINP) jets to reduce the wave drag and heat flux of bodies in supersonic and hypersonic flows. More

[1]Corresponding Author: Email: mbarzegarg@yahoo.com, Phone: +98 9112159133, Fax: +98 21 77240488.

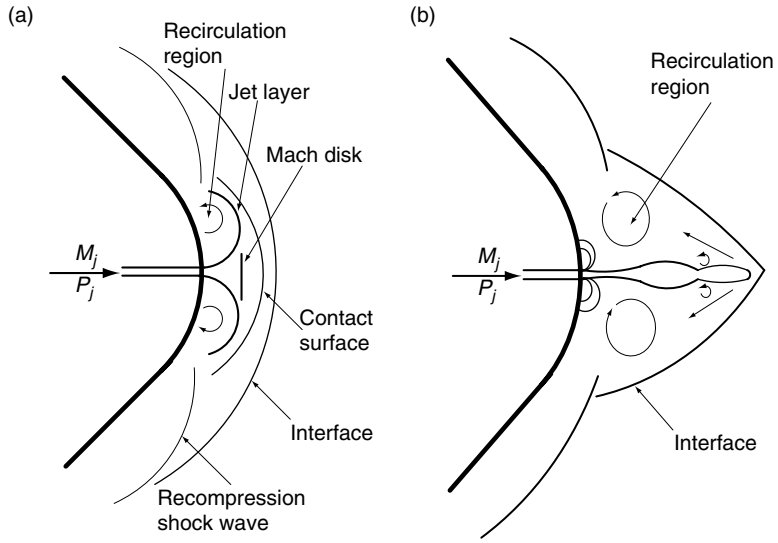

Figure 1. Schematic representation of the flow field features around the blunt cone with a counterflowing a) SPM jet b) LPM jet.

recent works [10–13] have revealed that various shock-dissipating and anomalous effects are produced by WINP jets in high-speed flows. These experiments also revealed short penetration mode (SPM) and long penetration mode (LPM) jets with LPM jets giving larger drag reductions and shock standoff distances. A schematic representation of the flow field features around the blunt cone with a counterflowing jet is showed in Fig 1. Shang et al. [11] and Shang [12] experimentally and computationally investigated the aerodynamic effects of various counterflowing jets, with and without plasma, to determine the amount of drag reduction in a hypersonic flow over a sphere.

The main objectives of the present study are 1) visualization of the shock structure around the blunt cone with varying coolant gas as the counterflow jet because of its valuable effect on heat reduction, 2) effects of different conditions of the counterflow jet on thermal protection, 3) Stanton distribution along the surface of the blunt cone 4) effects of LPM and SPM on the flow field in the vicinity of the blunt cone, and 5) performance of illustrative numerical simulations using computational-fluid-dynamics (CFD) codes to complement the experiments.

2. GOVERNING EQUATIONS AND NUMERICAL METHOD

The focus of this study is the final phase of the jet development near the exit field after complete transition to turbulence. High spatial and temporal resolution was used to resolve the unsteady structures of the flow and their effects on mixing with resorting to turbulence modeling. Since the flows considered have large density variations, the averaged form of the Navier Stokes equations were used as the following:

Conservation of mass:

$$\frac{\partial \rho}{\partial t} + \vec{\nabla} \cdot (\rho \vec{\mathrm{V}}) = 0 \tag{1}$$

Conservation of momentum:

$$\frac{\partial \rho \vec{\mathrm{V}}}{\partial t} + \vec{\nabla} \cdot (\rho \vec{\mathrm{V}} \vec{\mathrm{V}}) = \vec{\nabla} p + \vec{\nabla} \cdot \bar{\bar{\tau}} + \rho \bar{g} \tag{2}$$

Conservation of energy:

$$\frac{\partial \rho E}{\partial t} + \vec{\nabla} \cdot ((\rho E + P)\vec{\mathrm{V}}) = \vec{\nabla} \cdot \left(k_{eff} \vec{\nabla} T - \sum_j h_j \vec{J}_J + \bar{\bar{\tau}}_{eff} \cdot \vec{\mathrm{V}} \right) \tag{3}$$

And the species transport equation:

$$\frac{\partial \rho Y_i}{\partial t} + \vec{\nabla} \cdot (\rho \vec{\nabla} Y_i) = \vec{\nabla} \cdot \vec{J}_\iota \tag{4}$$

where $\bar{\bar{\tau}}$ is the stress tensor, E is a modified total energy, Y_i is the mass fraction, and $\vec{J_l}$ is the diffusion flux of species i, respectively. These terms are given by:

$$\bar{\bar{\tau}} = \mu \left[-\tfrac{2}{3} (\vec{\nabla} \cdot \vec{\mathrm{V}}) \bar{\bar{1}} + (\nabla \vec{\mathrm{V}} + {}^{t} \nabla \vec{\mathrm{V}}) \right], \quad E = h - \frac{p}{\rho} + \frac{v^2}{2}, \quad \vec{J}_\iota = (\rho D_{i,m} + \frac{\mu t}{Sc_i}) \vec{\nabla} \cdot Y_i \tag{5}$$

where μ is the molecular viscosity, ρ is the density, $\bar{\bar{1}}$ is the unit tensor and Sc_t is the turbulent Schmidt number and μ_t is the turbulent viscosity. The flow simulation being axisymmetric, the velocity vector $\vec{\mathrm{V}}$ is thereafter decomposed into $\mathrm{V_x}$ and $\mathrm{V_r}$ components, which are the axial and radial velocities, respectively. Also J_i can be expressed in terms of the binary diffusion coefficient $D_{i,m}$ and is defined by Fick's law. It states that if a species of molecular weight $\boldsymbol{M}_A$ is mixed with another species of molecular weight $\boldsymbol{M}_B$ at certain pressure and temperature, then $D_{i,m}$ can be defined as

$$D_{i,m} = 0.0018583 \frac{\sqrt{\overline{T^3} \left(\frac{1}{M_A} + \frac{1}{M_B} \right)}}{\bar{P} d_{AB}^2 \Omega_{AB}} \tag{6}$$

where D_{AB} is in $\mathrm{cm^2\ s^{-1}}$, $\bar{P}$ and $\bar{\mathrm{T}}$ are the pressure and temperature of the species, Ω_{AB} is the collision integral parameter and is a function of $\mathrm{k_1}\bar{\mathrm{T}}/\varepsilon_{AB}$ with $\mathrm{k_1}$ being Boltzmann constant, and $\varepsilon_{AB} = \sqrt{\varepsilon_A \varepsilon_B}$ with ε_A and ε_B the characteristic energy interaction parameters for the species, $d_{AB} = (1/2)(d_A + d_B)$ with d_A and d_B as the molecular diameters for the species. All these parameters are computed for all the coolant gases injected at the nose of the model and are given in Table 1.

Table 1. Flow condition of free stream and coolant gases

	Unit	Free stream	Jet		
Gas		air	He	air	Co_2
Mach number		5.75	1, 2	1, 2	1
Total pressure	Bar	9.9	0.5–6	0.5–9	0.5–6
Total temperature	K	1600	300	200, 300, 400	300
Molecular weight	Kg/kg mol	28.97	4.003	28.97	44.01
Molecular diameter (d_A)	A^0	3.61	2.57	3.61	3.996
$\frac{\varepsilon_A}{k_1}$	K	–	10.2	97	190
Ω_{AB}		–	0.6436	0.9878	1.273
D_{ab}	$(cm^2\ s^{-1})$		1.22	0.283	0.1746

The simulations were performed using an implicit CFD code. This code employs a conservative, cell centered, control volume formulation. A second order upwind scheme was used to discretize both momentum and continuity equations with a coupled solver. The convective fluxes were treated using the Roe Flux-Difference Splitting Scheme, which has been shown to improve treatment and accuracy at shocks. Furthermore, mesh refinement was used to ensure proper resolution. Second order dual timestepping was used to advance the flow field in time. The jet was considered to be air, hydrogen and Co_2, with the pressure, temperature and density being coupled using the ideal gas law. The properties of the gas mixture (gas constant, heat capacities, etc.) were calculated using kinetic theory. The convergence criterion is based on the difference in density values, ρ, at any grid point between two successive iterations i.e. $|\rho^{n+1} - \rho^n| \leq 10^{-5}$, where n is the iteration index. In order to increase convergence, blunt cone without jet was solved for the first step. After the flow field of shock in the vicinity of the nose is formed, a counterflow jet is issued from the nose. When the jet flows from the nose it severely oscillates. After a few time steps, the jet flow forms a steady flow field, though some small fluctuations remain. This phenomenon will be completely discussed in the following sections.

In the present flow field, The Reynolds number is $e = 1.6 \times 10^6$, which is obtained based on the diameter of the blunt body and the parameters of the incoming flow. The Reynolds number is so high that it is satisfactory to consider that the returning jet flow and the recirculating flow are fully turbulent, which can be proved by experimental data, so the effects of turbulent flow must be taken into account. In this paper, classical SST (Shear-Stress Transport) turbulent flow model is adopted [14]. This model doesn't need special treatments for the near-wall grids and can better predict the separation of boundary layer.

3. COMPUTATIONAL DOMAIN AND GRID

The geometry of the nose cone is determined by the size of the experimental shape. The shapes are obtained from a major reference [4]. In all cases, the bore diameter of the jet hole is 2 mm. The size and geometry of the blunt cone used in the experimental test are depicted in Fig 2a.

The results presented in this paper correspond to a counterflow jet (He, air, Co_2) released from a vessel pressurized in the range of 0.5–9 bar. Various jet conditions such as different gases (He, air, Co_2), several Mach numbers and pressure ratios were applied to jet. The pressure level was chosen to produce a jet flow regime. The types of boundary conditions for the grid are defined as shown in Fig. 2b. Further discussion about boundary and initial conditions can be found in previous paper [2]. The properties given to the external domain are listed in Table 1.

For a blunt cone without angle of attack, the flow is assumed to be axisymmetric. Thus, only half of the geometry needs to be simulated. As it was shown in Fig. 2b, these types of grids are quadrilateral elements.

The quality of the mesh plays a significant role in the accuracy and stability of the numerical computation. One of the attributes associated with the mesh quality is aspect ratio. Therefore, aspect ratio was controlled not to exceed a normal range. In the present case, the gradients normal to the wall are much greater than those which are tangent to the wall. Consequently, the cells near the surface have high aspect ratios. Also, an extensive grid refinement study (mesh size from 150 × 140, 340 × 240 and 440 × 300) was conducted to determine grid independence in heat transfer to resolve the boundary layers. For this, Y^+ over the wall surface of the nose was kept below 0.1. After this refinement, approximately 82000 (340 × 240) cells have proven enough for the 2D axisymmetric domain.

4. SOLVER VALIDATION

In our previous paper [1–2], the solver validation was committed by comparing the results to an experimental test run of Menezes's [3]. In addition, the bow shock stand-off distance of the nose cone without jet was compared with analytical calculations for all investigated freestream conditions. Also, comparison heat flux over blunt cone in 2D axisymmetric and 3D shows that 2D axisymetric results are acceptable. Therefore, the 2D axisymmetric model, with its low run time, is preferably acceptable.

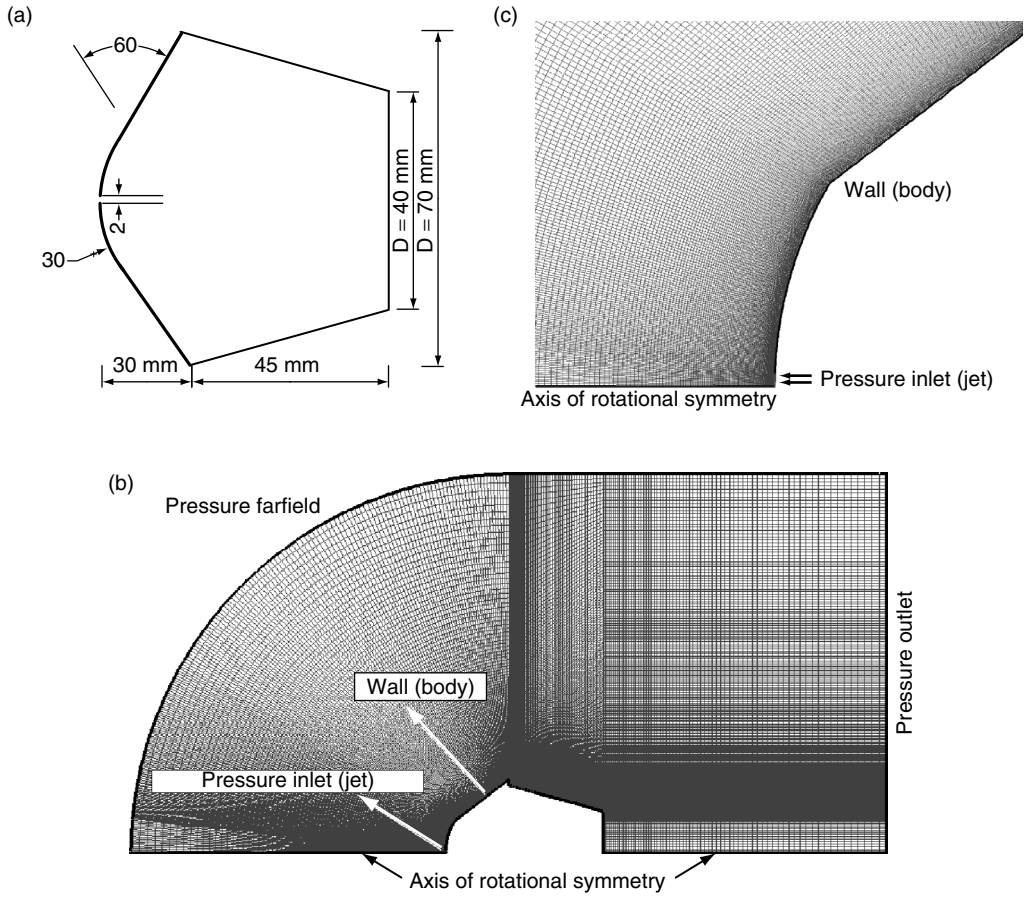

Figure 2. Geometry and Boundary condition types as defined for the simulations.

5. RESULTS AND DISCUSSION

When a jet issuing from a body interacts with supersonic/hypersonic incoming airstream, the body shock stands away from the body surface and takes a form appropriate to a new body consisting of the original body with a protrusion due to the jet flow. The boundary of the protrusion is defined by the interface, i.e., the stream surface between the jet flow and the mainstream flow. A model of jet and the interface flow is sketched in Fig. 1.

Daso [6] categorized the mode of jet penetration upon the flow rate or the driving nozzle stagnation pressure and therefore the type of nozzle expansion i.e., whether the jet was underexpanded, fully expanded, or overexpanded, based on the pressure difference between the nozzle exit total pressure and the static pressure of the ambient or shocked flow. However, Fomin [10] and Sahoo [4] classified these results with pressure ratio. They correlated the occurrence of the two modes with the stagnation pressure ratio parameter

$$PR = P_{tj} / P_{tf} \tag{7}$$

where P_{tj} is the total pressure of a jet and P_{tf} is the total pressure of free stream. It seems that pressure ratio can classify variations of different coolant gases more clearly and logically than other methods like the flow rate ratio.

For any outflow of the jet, P_{tf} was chosen greater than P_{tj} (PR < 1) to compare the result with main reference [4]. As the jet total-pressure ratio PR increases from its minimum value of 0.05, the bow shock moves forward. In general, this process is continuous, except for a small critical range of P where the trend is reversed. Below the critical range of P, the flow is observed to have more than one jet cell and is generally unsteady. Above the critical range, the flow is usually steady with a single jet cell terminated by a normal shock. The change from one type of flow to the other is intermittent in character. The estimated value of PR midway between the interception of transition and its completion is referred to as the critical value PR_{crit} and is primarily a function of the jet size, nose shape and coolant jet. Hence, the effectiveness of gas injection as a drag reduction or heat protection device is essentially dictated by the critical pressure ratio. Due to penetration of the jet into the main stream, the jet flow can create Long Penetration Mode (LPM) or Short Penetration Mode (SPM). The schematic flow field of each mode was illustrated in Fig. 1. Each mode has its own characters and properties. When the jet flow issues from the nose cone, LPM is a dominant mode in its vicinity. After the jet pressure increase, the LPM structure vanishes and SPM is the main mode. The critical pressure ratio which determines a jet mode depends on several factors like velocity and temperature of the jet and type of gas injection.

Figure 3 compares the flow field of various coolant jets (He and CO_2) with PR = 0.1 near the blunt cone. Since Helium has higher gas diffusivity than Carbon Dioxide (Table [1]), it penetrates more than CO_2 in the free stream (Fig. 3a). Hence, the mass species of helium is reduced in the vicinity of the nose cone. On the other hand, CO_2 has high molecular weight and it can't penetrate like Helium, but it fills the recirculation area around the nose. Therefore, the recirculation region of Helium is larger than Carbon Dioxide.

As it was shown in Fig. 3b, Mach structure around the nose cone is changed by various gases. Helium forms several Mach disks until it reaches the interface, but Carbon Dioxide only forms one Mach disk. Moreover, the temperature and streamline contours were shown in Fig. 3c and 3d. The temperature around these two gases is the same in general view, but the temperature in the vicinity of the interface is different.

In the reduction of aerodynamic heating, it is important to reduce the maximum value of the heat flux. Also, it is important to reduce the total heat load to the body. The total heat load Q is estimated as an integration of heat-flux distribution over the surface of the blunt body as follows:

$$q_w = h_f (T_f - T_w) \tag{8}$$

$$Q = 2\pi R^2 \int q_w \sin\theta \, d\theta \tag{9}$$

where h_f is the fluid-side local heat transfer coefficient. Hence, the evaluation of total heat load Q, based on Eq. (14), is considered accurate enough to discuss the difference of the total heat load because of opposing jets at various PR.

Also to compare the experimental and numerical results, the Stanton number was calculated over the body with respect to the nondimensional gauge locations (S/R_b) on the model surface at 0° angle of attack. The surface heat-transfer rates have been nondimensionalized in the form of Stanton number based on the free stream conditions given by the expression

$$S_t = \frac{q_w}{[\rho_\infty V_\infty C_{p\infty}(T_{aw} - T_w)]} \tag{10}$$

$$T_{aw} = T_\infty \left\{ 1 + \sqrt[3]{Pr_w} \left[(\gamma - 1)/2 \right] M_\infty^2 \right\} \tag{11}$$

where Pr_w is the Prandtl number set as 0.71.

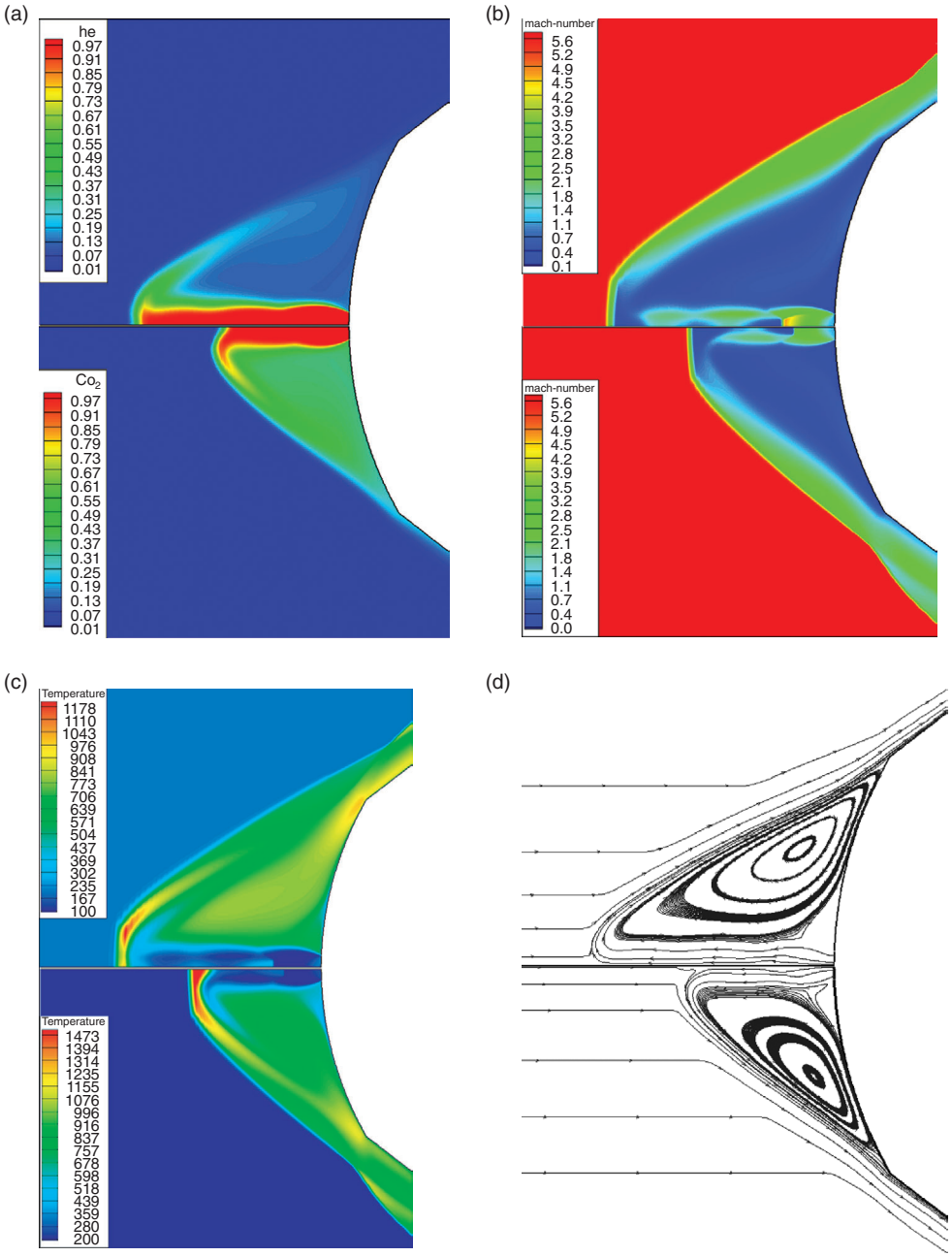

Figure 3. Comparison of flow field of Helium (upper) and Co_2 counterflowing jet in LPM (PR = 0.1).

5.1. *Effects of various coolant gas*

Effects of various coolant gases on heat load reduction were shown in Fig 4. In these cases, jet flow is sonic and pressure ratio changes from PR = 0.05 to Pr = 0.9. At the low pressure ratio (PR = 0.05, 0.1, and 0.15) i.e. the LPM, the counterflowing jet is seen to be nearly fully expanded, with the static pressure of the jet at the exit being, by definition, approximately the same as the static pressure of the ambient flow about the nozzle exit, consistent with the result of McGhee [13]. For the LPM jet flow

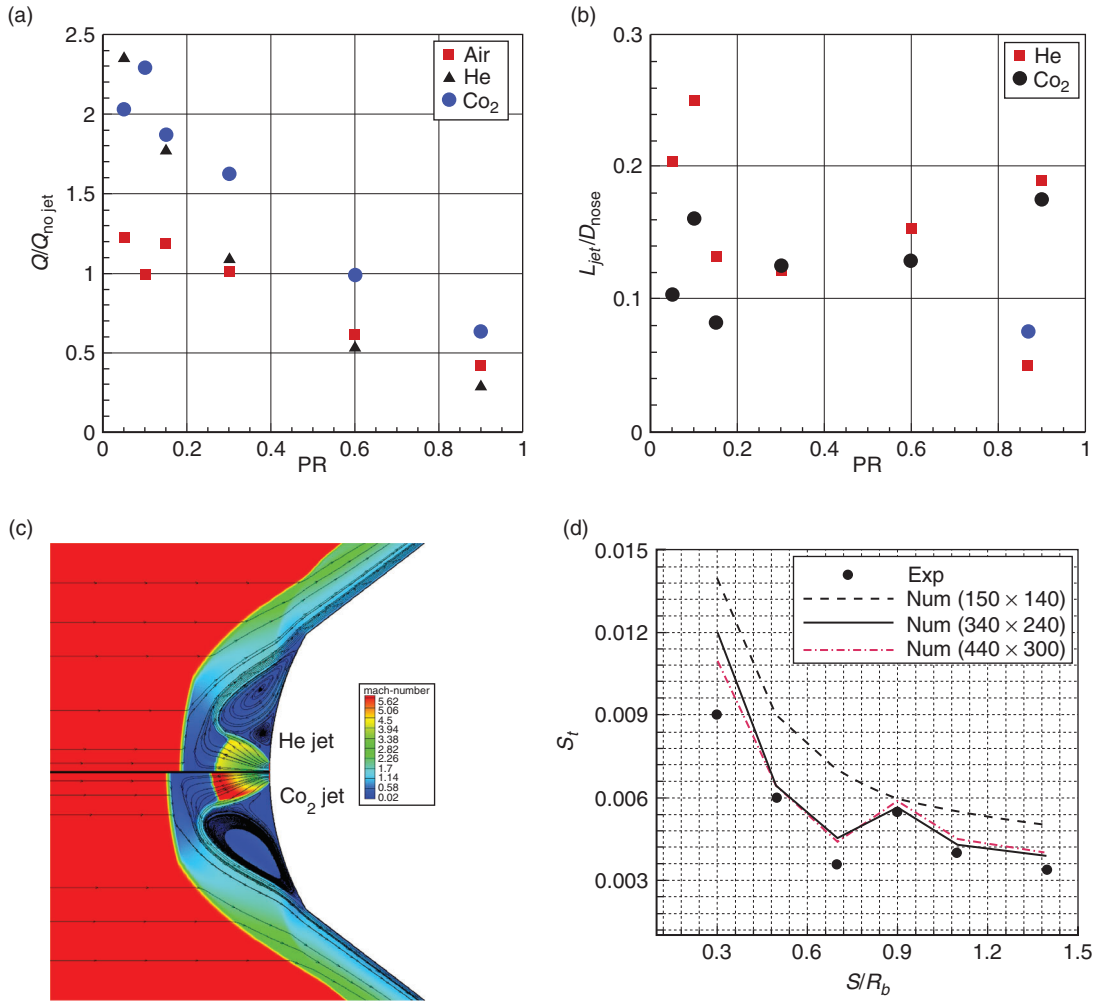

Figure 4. Comparison of effect of Helium (upper) and Co_2 counterflowing jet.

field, the flow structure reveals the shock to be so diffused or dispersed that it is no longer discernible, and thus the shock standoff distance could no longer be defined. To our knowledge, this degree of shock dispersion has only been observed in the schlieren images of McGhee [13], who identified three different flow regimes in the flow field of a Mach 3 freestream with a 140° cone with a centrally located Mach 3 "retronozzle" at 0°. If it can be sustained, such dispersion or dissipation of the bow shock of the model could have important applications in supersonic and hypersonic aerodynamics.

An equally important characteristic of the flow fields with LPM jets is the rather pronounced unsteadiness of the interactions at low jet flow rates, thrust, or mass flow coefficients and oscillation through a feedback mechanism. The unsteadiness and oscillations are quite evident in the schlieren figure and Mach contour of the numerical simulation.

Figure 4a illustrates the heat load reduction of various gas jets. In the case of PR < 0.4, the flow field is unstable, and the self induced oscillations of the bow shockwave are observed. Compared with the no-jet case, the heat flux is higher. Also, Hayashi [15] observed this phenomena in his result for free stream Mach = 4. Because the opposing jet does not form a stable flow field, it is quite unsteady. The body surface is not perfectly covered with the jet gas, and hot freestream gas sometimes reaches directly to the wall. Hence the heat-flux distribution is higher than that with no jet.

Various Coolant gases (He and CO_2) show different length of diffusivity due to their molecular weight at the same Mach number (Fig. 4b). As it was expected, Helium penetrates more than CO_2. At LPM criteria (PR < 0.15), helium shows an unsteadiness and fluctuation. After a sufficient increase in the pressure ratio, its characteristic properties seem similar to CO_2. Fig. 4c compares the Mach contour of Helium and CO_2 at PR = 0.6.

At the high Pressure Ratio (PR = 0.3, 0.6 and 0.9) the heat load shows consistent reduction with increasing pressure ratio. In this range, the SPM flow field seems dominant and the jet flow tends to be in the vicinity of the nose. Thus, Helium jet reduces more heat load than other gases.

Figure 4b also reveals dramatic changes in the flow structure and dynamics of the interaction as the counterflowing jet pressure ratio is increased above PR = 0.4. For PR = 0.3, the flow structure has transitioned from LPM to SPM. The schlieren videos show a sudden transition as the LPM jet jumps to SPM at some critical flow rate to instantaneously reestablish a weaker bow shock, with longer standoff distance compared to the baseline and a concomitant reduction in jet penetration. This sudden transition is referred to as bifurcation in some previous work [11]. We have, however, chosen not to identify the transition as bifurcation due to multiple meanings or interpretations of the word in describing other flow phenomena.

Figure 4c shows different flow features of the flow field for the SPM jet. In SPM, the jet is delineated by a barrel shock, capped with a terminal spherical shock downstream of the bow shock, with an interface located about midway from either shock. A supersonic jet stream emanates at the corner where the terminal shock and the jet barrel shock interact. This phenomena occur when an isolated shock generator for the incident shock is absent for the freestream-counterflowing jet interaction. The jet stream stagnates or impinges on the surface of the model and forms a stagnation circle, giving heat loads greater than the case without injection. The stagnation ring location on the surface moves radially out with increasing flow rate or jet stagnation pressure (Fig. 4b). At even higher flow rates, the jet stream is seen to clear the face of the model, relieving the dilemma of increased heating. Also, it is quite noticeable that the pocket of separated flow in the baseline flow field has disappeared with counterflowing jet injection as a lower pressure region becomes established in the model face.

Also, the Stanton number was calculated over the surface of the blunt cone in order to validate the numerical simulations and evaluate mesh independency. Fig. 4d compares the Stanton number over the nose surface with CO_2 jet. Comparisons show a good agreement between numerical and experimental results and mesh quality (340 × 240) seems appropriate and enough for comparison.

5.2. *Effects of Jet Total Temperature*

The effects of total temperature of opposing jets are investigated for air jet. The total temperature of the jet is changed with the same total pressure ratio (PR = 0.05, 0.1, 0.15, 0.30, 0.60). Also, by fixing the Mach number on a unity value for the inlet jet, the mass flow ratio changes with changing total temperature.

Figure 5a shows a heat load reduction for various total jet temperatures. At low pressure ratio (PR < 0.15), it seems that the unsteady structure of the jet does not show any specific trend. When the pressure ratio increases, the heat load shows expectable reductions. In high pressure ratios, the heat load reduces significantly. This reduction is due to low temperature flow fields in the recirculation region as it was shown in Fig. 5a.

Figure 5b illustrates the temperature and streamline of flow field around the nose cone. With the equation of state $P = \rho RT$ and the assumption that the pressure is equal in both cases, it results that density increased when temperature is reduced. Moreover, the strength of recirculation is dependent upon density with the equation $\varphi = \int \rho\ u\ dA$. Thus, when the temperature of the jet is reduced, recirculation in the vicinity of the nose cone becomes stronger and heat load over the blunt cone is reduced (Fig. 5).

5.3. *Effects of Jet Gas Diffusivity*

Figure 6 illustrate the effects of binary diffusion coefficient ($D_{i,m}$) on heat load reduction for different pressure ratios (PR = 0.1, 0.3, 0.6 and 0.9). At low pressure ratios (PR = 0.1), oscillation due to unsteady structure of flow seems dominant and the results prove this idea. However, when the pressure

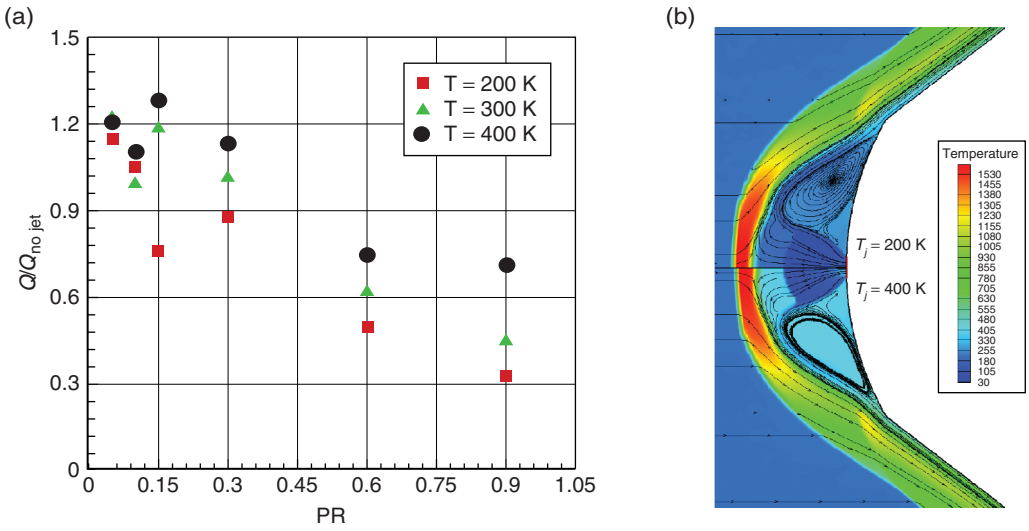

Figure 5. effects of temperature on (a) Heat Load reduction (b) flowfield around nose cone (PR = 0.6).

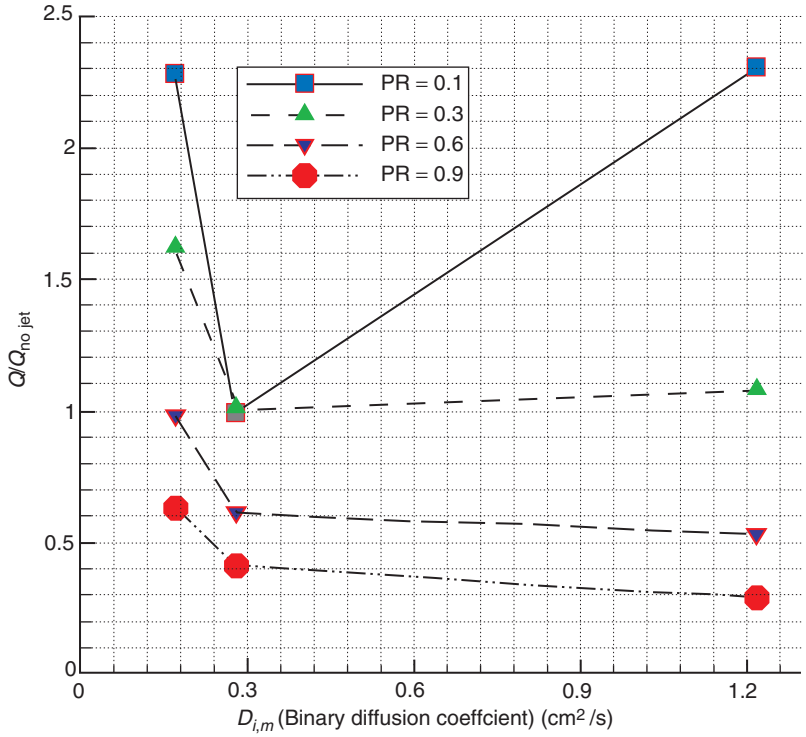

Figure 6. Comparison of effects of Binary Diffusion Coefficient on Heat Load reduction for various Pressure Ratio (Mach = 1).

ratio is increased, variations of heat load show a logical trend. Generally, when a lighter injected gas like Helium comes out of the exit plane, it expands much faster along the surface of the body. At low pressure ratios, it penetrates into the main stream and does not create any recirculation region in the vicinity of the nose cone. Moreover it may cause a high temperature region near the nose and may increase the heat load (as it was shown in Fig. 6 for PR = 0.1). So the cooling effect is reversed and

only felt at the further part of the surface [Menezes]. For a heavier gas, in particular, Carbon Dioxide, the diffusion takes place much faster near the stagnation region but it cannot cause any reduction in the flow field around the nose cone. Hence, it is concluded that the cooling performance with either heavier gas injections with low $D_{i,m}$ or lighter gas injections with high $D_{i,m}$ is not profitable close to the stagnation region for the low pressure ratio condition. However, When the pressure ratio is increased (Pr = 0.6 and 0.9), it seems that the lighter gas with high binary diffusion coefficient creates a recirculation region near the nose cone and reduces the heat load over the blunt cone. Therefore, cooling effects of helium in high pressure ratios are significantly greater than the effects of Carbon Dioxide due to high diffusion coefficient.

5.4. *Effects of Jet Mach Number*

Figure 7 illustrates the effects of the Mach number on heat load reductions. The jet Mach number can influence the flow around the nose cone in two ways. Firstly, it can change the range of LPM and SPM for the jet. As it was shown in Fig. 7a, at low pressure ratios, there is not much difference between

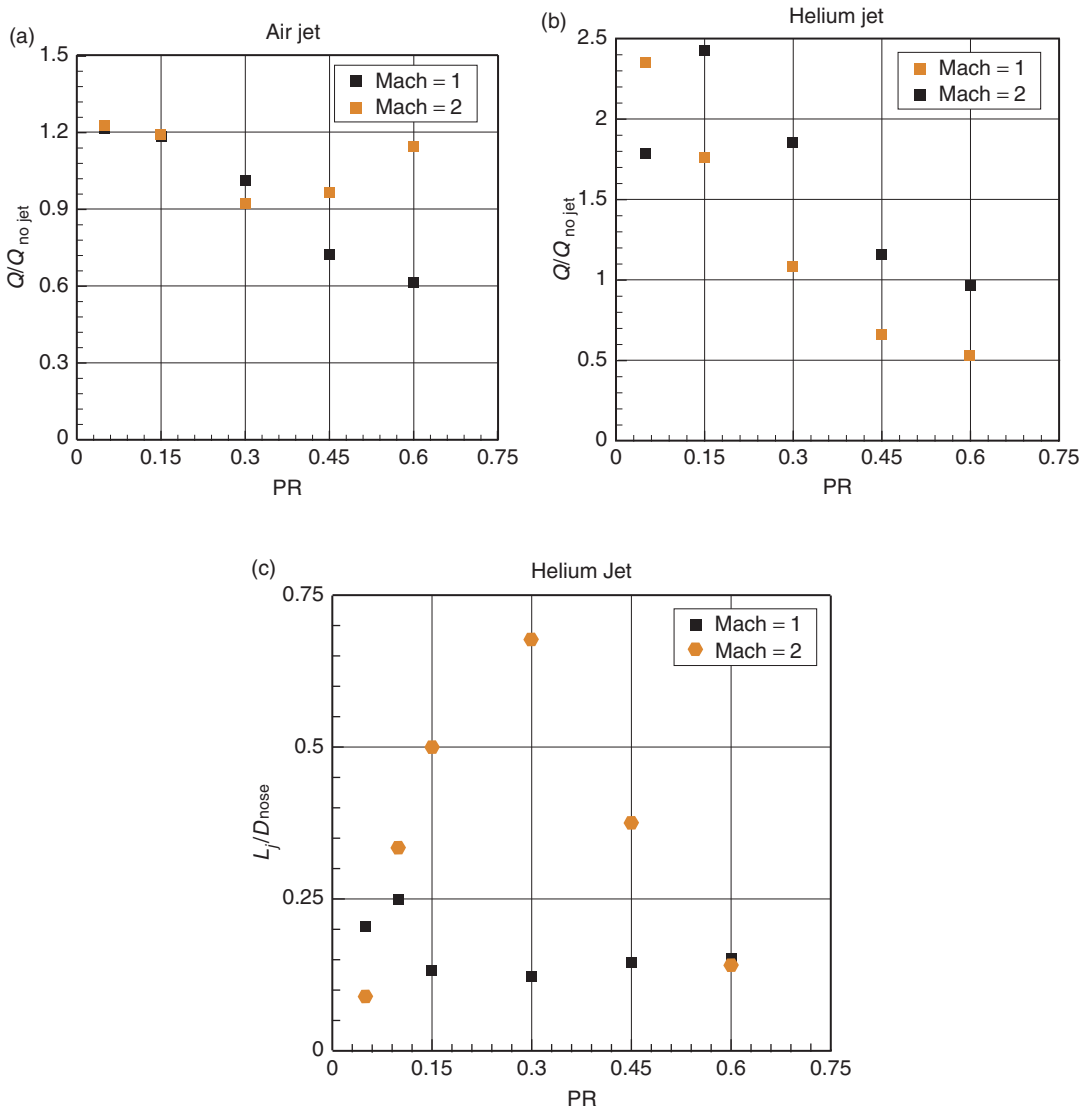

Figure 7. comparison of mach of jet on (a) Heat Load reduction in air (b) Heat Load reduction in air (c) jet penetration length.

various Mach numbers. After an increase in the pressure ratio to values more than 0.3, the jet flow structure with Mach = 2 changes and it penetrates into the main stream and several shock interfaces are created. Hence, the jet flow becomes LPM. In this situation, further increase of pressure ratio does not reduce heat load because of the LPM structure of the jet. On the other hand, the air jet with unit Mach number preserves its SPM structure despite low velocity. Also, its cooling effects increase with increasing pressure ratios. This reduction in heat load is due to their recirculation area in the vicinity of the nose cone.

For Helium jet, Mach number influence is in a same trend, but with a different range. Due to high binary diffusion coefficients (low molecular weight), the LPM structure occurs at low pressure ratios. When the jet Mach number is unity, the LPM structure changes to SPM with increasing the pressure ratio to values more than 0.15. Thus, further increase in pressure ratio increases the recirculation region and reduces the heat load. This change in LPM and SPM structure can be measured by the length of the jet as it is shown in Fig. 7c. The length of the jet is defined by the length where the helium jet mass fraction is less than one percent. This figure (Fig. 7c) clearly shows the LPM range for various Mach numbers. It seems that the LPM structure reaches its maximum penetration in PR = 0.1 for Mach = 1. On the other hand, the Helium jet with mach = 2 reaches to a maximum jet length value in PR = 0.3.

Thus, the LPM jet occurs for both the sonic and supersonic jets, with the degree of penetration depending upon the jet nozzle exit Mach number and Gas diffusivity (Fig. 7c).

5. CONCLUSION

The film cooling effectiveness of the injection of various coolant gases from the stagnation zone of a hypersonic blunt body has been numerically investigated and a comparison has been made between their reduction percentages in heat load. Essentially, the effect of pressure ratio of the jet for various Mach numbers, jet temperature (varying total temperature), and the molecular weight of each coolant gas on the film cooling performance is investigated. The following conclusions are made from these results.

1. It is observed that the cooling performance of the jets with low pressure ratio is not efficient and the unsteady structure of the jet changes its flow and performance.
2. The lighter gas, Helium, is found to have a better cooling performance than Carbon Dioxide in high pressure ratios. The cooling performance of helium due to its binary diffusivity character is efficient in increasing the performance of the recirculation region. In fact, configuration of jet which was release from nose cone simulate spike that improve the performance of this device.
3. The increase in pressure ratio, which essentially increases the mass flow rate and create better jet configuration , generally leads to better cooling performance, and less jet unsteadiness.
4. The unsteadiness in the heat transfer value with coolant injection is mainly due to the unsteadiness in the boundary layer filled with coolant mass, as the external flow is steady as seen from the visualizations. Moreover, unsteady structure of jet is reduced when Pressure Ratio increases and jet structure seems more stable.
5. Low total jet temperature undoubtedly helps the cooling performance of the jet and the recirculation region.
6. Jet structure play crucial rule in cooling performance of counterflowing jets. In high Pressure Ratio, the formation of jet creates structure that main flow doesnot receive to blunt body and the recirculation region near blunt body can vent from the tip of edge. This phenomenon greatly affect on the cooling performance of counterflowing jet.

These results suggest that applying counterflowing jets can influence on hypersonic vehicle design and performance, like encountered in augmenting thermal protections to significantly reduce the high risks associated with planetary atmospheric entry and reentry.

REFERENCES

[1] M. Barzegar Gerdroodbary, S.M. Hosseinalipour, Numerical simulation of hypersonic flow over highly blunted cones with spike, Acta Astronautica, 67, (2010) 180–193.

[2] M. B. Gerdroodbary , Shervin Bishesari, S. M. Hosseinalipour, K. Sedighi, Transient Analysis of Counterflowing Jet over Highly Blunt Cone in Hypersonic Flow, Acta Astronautica, 73, (2012) 38–48.

[3] V. Menezes, S. Saravanan, G. Jagadeesh, K.P.J. Reddy, Experimental investigations of hypersonic flow over highly blunted cones with aero-spikes, AIAA Journal 41 (2003) 1955–1966.

[4] N. Sahoo, V. Kulkarni, S. Saravanan, G. Jagadeesh, and K. P. J. Reddy, Film cooling effectiveness on a large angle blunt cone flying at hypersonic speed, Phys. Fluids **17**, 036102, 2005.

[5] Vinayak Kulkarni, K. P. J. Reddy, Counterflow Drag Reduction Studies for a Blunt Cone in High Enthalpy Flow, International Journal of Hypersonics, Vol. 1, No.1, 2010, pp. 69–76.

[6] Endwell O. Daso, Victor E. pritchett, Ten-See Wang, Dale K. Ota, Isaiah M. Blankson, Aaron H. Auslender, Dynamic of Shock dispersion and Interaction in Supersonic Freestreams with counterflowing jets, AIAA Journal, Vol. 47, No. 6, 2009, pp. 1313–1326. doi:10.2514/1.30084.

[7] M. Gauer, A. Paull, Numerical Investigation of a Spiked Blunt Nose Cone at Hypersonic Speeds, Journal of Spacecraft and Rockets, Vol. 45, No. 3, 2008, pp. 459–471. doi:10.2514/1.30590.

[8] Prasad S. Srinivas, R.K. Sharma, Dr., D.K. Yadav, G.V. Ramana Murty, CFD Analysis of the Aerodynamic Interaction Effects Due to Lateral Jet Injection in to Hypersonic Flow, International Journal of Hypersonics, Vol. 1, No.1, 2010, pp. 135–144.

[9] S. Srinath, K. P. J Reddy, Experimental Investigation of the Effects of Aerospike Geometry on Aerodynamic Drag and Heat Transfer Rates for a Blunt Body Configuration at Hypersonic Mach Numbers, International Journal of Hypersonics, Vol. 1, No.1, 2010, pp. 93–114.

[10] V. M. Fomin, A. A Maslov, N. D. Malmuth, V. P. Fomichev, A. P. Shashkin, T. A. Korotaeva, A. N. Shiplyuk and G. A. Pozdnyakov, Influence of Counterflow Jet on Supersonic Blunt-Body Pressures, AIAA Journal, Vol. 40, No. 6, June 2002, pp. 1170–1177. doi:10.2514/2.1768.

[11] J. S. Shang, J. Hayes, K. Wurtzler, and W. Strang, jet Spike Bifurcation in High Speed Flows, AIAA Journal, Vol. 39, No. 6, June 2001, pp. 1159–1165.

[12] J. S. Shang, Plasma Injection for Hypersonic Blunt-Body Drag Reduction, AIAA Journal, Vol. 40, No. 6, June 2002, pp. 1178–1186. doi:10.2514/2.1769

[13] R. J. McGhee, Effects of a Retrorocket Located at the Apex of a 140' Blunt Cone at Mach Numbers of 3.00, 4.50, and 6.00, NASA TN D- 6002, Jan. 1971.

[14] F. R. Menter, M. Kuntz, R. Langtry, Ten Years of Experience with the SST Turbulence Model, Heat and Mass Transfer 4, pages 625–632, Begell House Inc, 2003.

[15] K. Hayashi, S. Aso, T. Tani, Numerical Study of Thermal Protection by Opposing Jets, AIAA Paper 2005–188, Jan. 2005.